ADVANCED FUNCTIONAL MATERIALS
www.afm-journal.de

Silicon Nanocrystals in Liquid Media: Optical Properties and Surface Stabilization by Microplasma-Induced Non-Equilibrium Liquid Chemistry

Davide Mariotti, Vladimir Švrček, Jeremy W. J. Hamilton, Michael Schmidt, and Michio Kondo*

Surface engineering of silicon nanocrystals directly in water or ethanol by atmospheric-pressure dc microplasma is reported. In both liquids, microplasma processing stabilizes the optoelectronic properties of silicon nanocrystals. The microplasma treatment induces non-equilibrium liquid chemistry that passivates the silicon nanocrystals surface with oxygen-/organic-based terminations. In particular, the microplasma treatment in ethanol drastically enhances the silicon nanocrystals photoluminescence intensity and causes a clear red-shift (≈80 nm) of the photoluminescence maximum. The photoluminescence properties are stable after several days of storage in either ethanol or water. The surface chemistry induced by the microplasma treatment is analyzed and discussed.

1. Introduction

Silicon nanocrystals (SiNCs), or silicon quantum dots, are nanoscale structures with typical diameters below 10 nm that exhibit quantum confinement effects. The combination of SiNCs unique characteristics produces a set of very interesting properties that are scientifically intriguing, experimentally challenging, and technologically very promising.[1–9]

Silicon, which is an indirect bandgap material, is subjected to drastic changes in its energy structure when confined to sub-5 nm dimensions: widening of the indirect bandgap, reduction of the direct bandgap, reduced efficiency in phonon-assisted transitions, and multi-exciton generation are some of the properties that have resulted from theoretical and/or experimental investigations.[1,4–6,8,10] These properties suggest the possibility of using silicon for efficient optoelectronic conversion with potential applications in photonics,[5,11] medicine,[2,12,13] and photovoltaics (PVs).[14–17] A range of synthesis techniques have been devised[18–25] and have contributed to clarify many aspects of these promising nanoscale structures. However, there is still limited control over the synthetic capabilities and in particular methods for engineering the surface characteristics are required.

Control of SiNCs surface properties is crucial for a complete understanding of SiNCs behavior and for their successful integration in application devices. The combination of quantum effects due to a reorganized energy structure and the possibility of various surface terminations can largely complicate the interpretation of experimental results and therefore it is essential that accurate control of the physical properties is achieved. Furthermore, engineering of the SiNCs surface is fundamental to achieve technologically viable devices that rely on efficient electronic transport across the SiNCs outer interface. For instance organic stabilization has shown promising results for preserving the properties of SiNCs;[7,23] however long organic molecules can prevent efficient exciton dissociation, which is required for PV applications. Processability is another aspect that needs to be considered and the possibility of manipulating SiNCs in colloids is of great interest and has recently shown potential advantages for next generation and low-cost solar cells.[14,16] The key objective is therefore to achieve understanding and superior control over SiNCs surface chemistry.

In this context, our recent work has focused on identifying methodologies for surface engineering to achieve stable oxygen-based passivation and/or organic-/carbon-based terminations of a few atomic layers and that would still allow successful integration of SiNCs in PV devices.[14,17,26–32] In particular, we have shown that nanosecond laser[14] and dc atmospheric-pressure microplasma processing[29] can successfully produce SiNCs with stable properties in liquid media. We have also observed that surface chemistry has also great influence on the post-processing interactions among SiNCs[27] and can induce self-organization in long-range conductive networks,[26,29,31] which can be useful to produce percolating networks in bulk heterojunction solar cell architectures.

D. Mariotti, J. W. J. Hamilton
Nanotechnology & Integrated Bio-Engineering Centre (NIBEC)
University of Ulster
Newtownabbey, BT37 0QB, UK
E-mail: d.mariotti@ulster.ac.uk
V. Švrček, M. Kondo
Research Center for Photovoltaic Technologies
National Institute of Advanced Industrial Science and Technology (AIST)
Tsukuba, 305-8568, Japan
M. Schmidt
Electron Microscopy and Analysis Facility
Materials Chemistry and Analysis Group
Tyndall National Institute
University College Cork
Lee Maltings, Cork, Ireland

DOI: 10.1002/adfm.201102120

The use of atmospheric-pressure plasmas is very attractive for industrial exploitation as these can drastically lower the costs and increase production throughput.[22,33–35] Although a range of challenges still need to be overcome, atmospheric pressure plasmas have gained momentum and are being increasingly applied to nanofabrication, deposition of advanced and functional coatings, and also for a range of other applications.[22,26,33–40]

2. Results and Discussion

In this contribution we investigate the properties and surface characteristics of electrochemically etched SiNCs that have been dispersed in water or in ethanol. We show that changes in surface chemistry at room temperature in water or ethanol are responsible for decreasing the photoluminescence (PL) intensity, degrading the optical properties. We then discuss SiNCs surface engineering by atmospheric-pressure microplasma-induced non-equilibrium liquid chemistry (MiNE-LC) directly in water or in ethanol. The microplasma process is capable of stabilizing SiNCs properties in ethanol producing a PL red shift of almost 80 nm; microplasma processing of water-SiNCs colloids produces different results with increased PL intensity but a minimal red-shift (≈12 nm). MiNE-LC is discussed and supported by PL measurements, transmission electron microscopy (TEM), and Fourier transform infrared (FTIR) spectroscopy.

2.1. Characteristics of Electrochemically Etched Si Nanocrystals (SiNCs)

Electrochemical etching produces a porous top layer on a silicon substrate, where the porous layer is formed by nanosized silicon crystals, i.e., SiNCs. A powder containing single SiNCs and SiNCs clustered in larger aggregates (up to micrometer size) can be easily obtained by mechanically removing the porous layer from the single crystal silicon substrate.[18]

SiNCs produced by electrochemical etching are for the most part terminated by hydrogen atoms[41] and it is well established that the processing conditions (current, electrolyte composition, wafer doping, etc.) can be used to control the porosity of the porous silicon layer and therefore determine the size of the SiNCs.[41,42] The effect of processing conditions on the degree and type of surface passivation is less discussed in the literature. A comparison of results reported in the literature[4,7,43–45] can reveal that SiNCs produced by electrochemical etching at different conditions can lead to quite dissimilar properties originating from diverse surface chemistries, even before SiNCs are exposed to air or any other post-synthesis environment (see Supporting Information for more details on the effects of electrochemical etching conditions). In addition to H-terminations, electrochemical etching can produce Si-dimers and possibly silicon dangling bonds where the respective degree of surface coverage strongly depends on electrolyte composition as well as the applied current density.

In our case, the applied current density is relatively low (compared to similar reports[7,45]) and therefore we expect a relatively large coverage of hydrogen passivation with some degree of Si-dimers being still present. The H-terminations are relatively stable at room temperature and can be desorbed only for temperatures well above 500 K,[43,46,47] therefore oxidation in air can only proceed through oxygen or water vapor cleavage of exposed surface Si–Si bonds[48] or direct passivation of Si dangling bonds. For instance water molecules can dissociate on the Si–Si bonds producing Si–H and Si–OH terminations.[48] Pairs of adjacent Si–OH terminations can then condensate releasing water and passivating the surface with the formation of Si–O–Si or Si=O bonds.[48] All this can happen, while H-terminations remain stable in air.

Dry SiNCs surface characteristics as discussed above are confirmed by FTIR analysis (**Figure 1**); the SiNCs powder was stored in ambient air at ambient temperature for several months (see Supporting Information for more details on the SiNCs stability in air). Si–H bonds produce a characteristic absorption band between 2050 cm^{-1} and 2150 cm^{-1} where the different peaks correspond to SiH, SiH_2, and SiH_3. In Figure 1a, the lowest absorption is due to trihydrides around 2130 cm^{-1}, at about 2110 cm^{-1} both SiH and SiH_2 contributed to the absorption signal, and finally at about 2090 cm^{-1} SiH is responsible for the absorption peak (see ref. [47,48] for more specific assignments). SiH_x absorption is also present between 600 cm^{-1} and 700 cm^{-1} with characteristic peaks at 626 cm^{-1} and 667 cm^{-1}; however in this case the assignment is not specific to any particular hydride.[48] Si–H stretching specifically from SiH_2 is also responsible for absorption at about 916 cm^{-1}.[49] Therefore, dry SiNCs produced for this work have clear hydrogen terminations

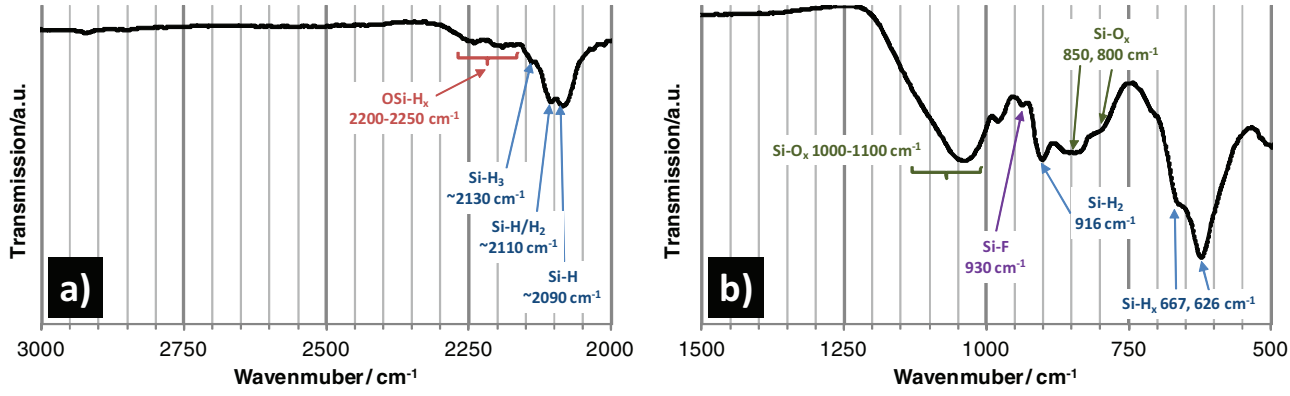

Figure 1. FTIR transmission signal of the dry SiNC powder produced by electrochemical etching and subsequent mechanical pulverization. The powder was exposed to ambient air and ambient temperature for several months. a) FTIR signal from 3000 cm^{-1} to 2000 cm^{-1} and b) FTIR signal of the same sample in the range 1500–500 cm^{-1}.

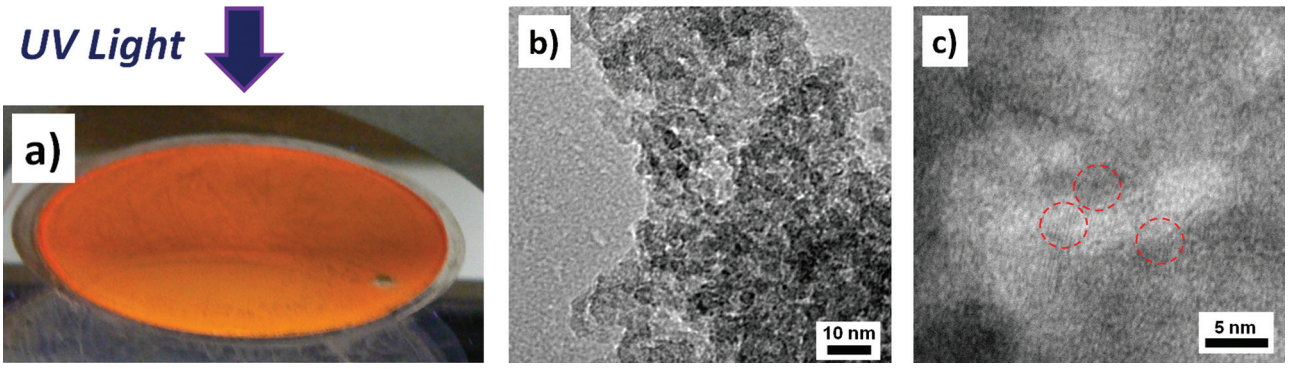

Figure 2. a) Photograph of electrochemically etched silicon wafer under UV exposure at 365 nm showing orange photoluminescence. Low resolution (b) and high-resolution (c) TEM images of SiNC powder prepared by electrochemical etching and used in this study. SiNCs that exhibit crystal fringes have been circled in red in (c) where the crystal size can be estimated to be below 5 nm diameter.

and assuming that the absorption coefficient is comparable for all the SiH_x contributions, silicon dihydrides appears to be the most frequent type of termination if compared to SiH and SiH_3.[48] The peak at 930 cm^{-1} is attributed to Si–F bonds, which may be a consequence of HF etching; this absorption feature has been observed before[50] and we have been unable to associate this to any other relevant chemical bond. The absorption related to Si–O–Si bonds is found between 1000 cm^{-1} and 1100 cm^{-1},[51] at 800 cm^{-1},[52] and 850 cm^{-1}.[48] The main absorption 1000–1100 cm^{-1} has large absorption coefficient[43] and therefore Figure 1b suggests a limited degree of oxidation. Limited SiNCs surface oxidation is also in agreement with the low absorption attributable to monohydrides, which indicates limited Si-dimers $(SiH)_2$ surface terminations[43] and confirms that oxidation proceeded mainly through cleavage of Si–Si bonds and direct passivation of dangling bonds. It is true that porous silicon can be oxidized in air to a certain degree; however, the rate is quite slow due to the stabilization effects of the H-terminations.[43] The peak shifted towards 1050 cm^{-1} as opposed to 1075 cm^{-1} for Si–O–Si stretching is a clear indication of non-stochiometric oxide.[50,51] The broadening of the 1000–1100 cm^{-1} band is a manifestation of the statistical distribution of different bonding arrangements at each silicon atom site.[51] Finally absorption between 2200 cm^{-1} and 2250 cm^{-1} are attributed to Si–H stretching with back-bond oxidation and the low absorption signal can be interpreted as the oxidation process being contained within a few outer monolayers of the SiNCs at the expense of both dangling bonds and Si-dimers that were exposed to air.

Photoluminescence properties of porous silicon can be easily observed under UV illumination at 365 nm (**Figure 2**a) while the SiNCs crystal structure has been analyzed by TEM. Figure 2b,c show lower and higher magnification TEM images of the SiNCs powder with some SiNCs showing typical fringes of crystalline materials for particles with diameter below 5 nm.

2.2. Effect of Water and Ethanol on the SiNCs Optical Properties

Separate colloids of water/SiNCs (W/SiNCs) and ethanol/SiNCs (Et/SiNCs) were produced by adding the SiNCs powder (5 mg) in 20 mL of water or ethanol. Because SiNCs are highly hydrophobic, a few drops of ethanol have been added to the water-based colloid (W/SiNCs) to wet the SiNCs surface (see Supporting Information for more details about the hydrophobicity of SiNCs in water). In order to remove the largest aggregates, the colloids were left to settle for 15 min and the supernatant parts were used to produce two 10 mL samples, one W/SiNCs and one Et/SiNCs. Shortly after dispersion in water or ethanol, SiNCs exhibit PL properties as shown in **Figure 3**a,b (green lines labeled as-prepared).

Our observations, shortly after dispersion, systematically show higher PL intensity for the W/SiNCs compared to the Et/SiNCs (Figure 3a,b; green lines labeled as-prepared), while the PL peak wavelength is the same for both colloids and located at about 600 nm. Higher PL intensity for the W/SiNCs is likely due to a rapid oxidation process that takes place when SiNCs are in contact with water as it will be discussed further below, while in ethanol this process does not occur or it is slower due to the presence of dissolved water vapor from air (see Supporting Information for details on the presence of water traces in ethanol). The broad PL spectra originate from the size distribution for quantum confined SiNCs with diameter below 10 nm.

In order to investigate the effects of ethanol and water on the SiNCs we have monitored the PL of the two colloids for several days and similar PL characteristics were revealed (Figure 3). Figure 3 shows PL spectra of SiNCs dispersed in water (a) and ethanol (b) stored in ambient conditions and measured at different times. Figure 3c,e summarize the PL intensity and PL maxima wavelength of W/SiNCs and Figure 3d,f summarize corresponding PL characteristics for the Et/SiNCs.

As previously mentioned, electrochemically etched porous silicon generally produces H-terminated silicon surfaces and it is not uncommon to find Si-dimers and dangling bonds.[4,7,43–45,53] Prior to dispersion in water/ethanol, the powder is exposed to air, which can contribute to oxidation as was previously discussed and confirmed by FTIR analysis of Figure 1. Therefore after exposure to air, the SiNCs powder presents stable Si–H and oxygen-based surface terminations with $(SiH)_2$ dimers that may be still present depending on the humidity level and the time that the SiNCs have been left exposed to air (see Figure 1 and Supporting Information about the stability of SiNCs stored in ambient conditions).

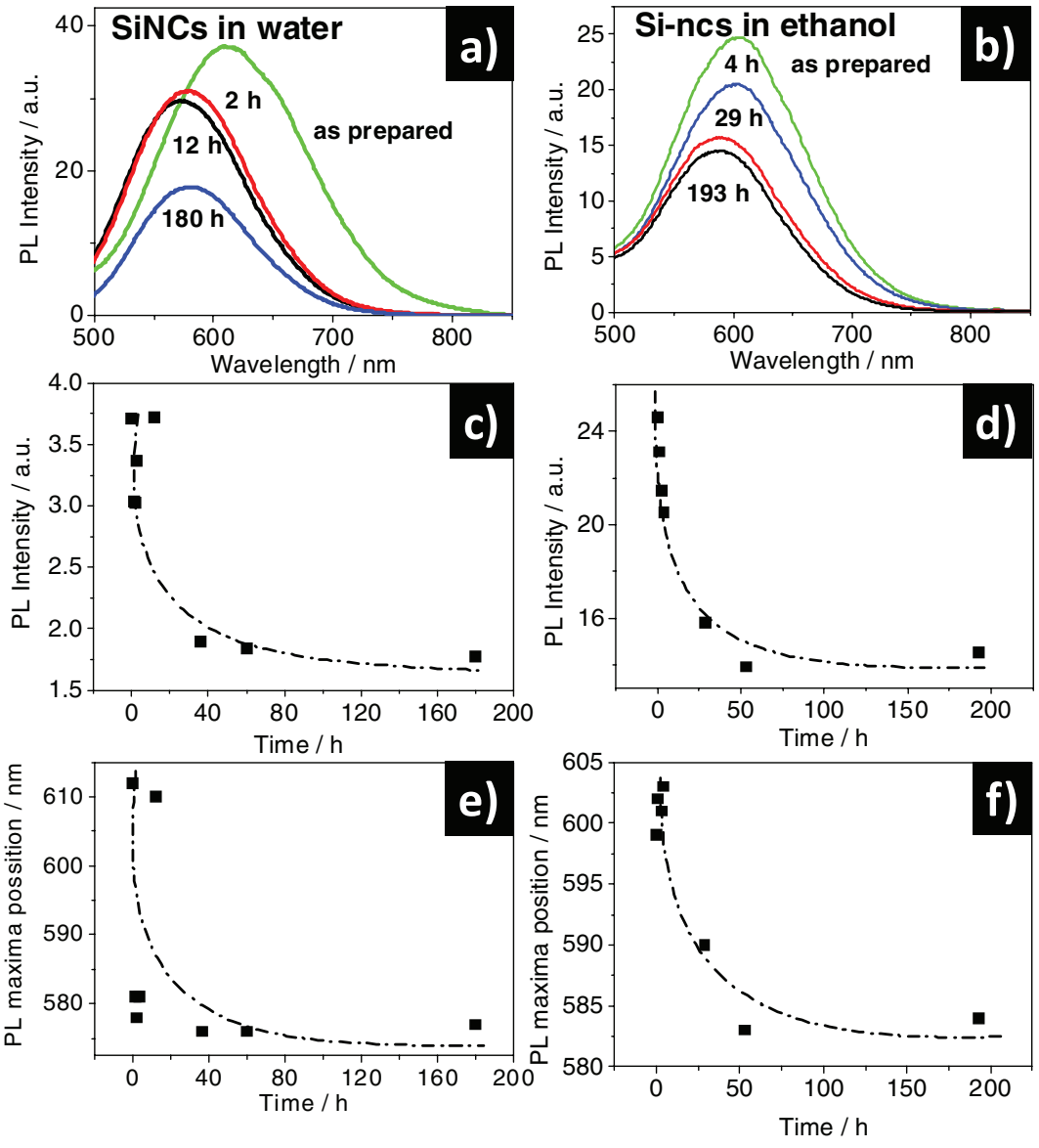

Figure 3. PL spectra of SiNCs dispersed in water (a) and in ethanol (b) stored in ambient conditions for different number of hours. Summary of PL intensity (c,d) and PL maxima (e,f) of the colloids as a function of time: c,e) represent PL properties for SiNCs dispersed in water and d,f) are the corresponding PL properties for the ethanol/SiNCs colloid.

The dispersion of the powder in liquid provides the opportunity to reinitiate and accelerate the surface chemistry by involving H-terminations, which instead remained unaltered when exposed to air. In water, OH^- ions can quickly replace H-terminations that were instead stable in air and the condensation process (that produces surface oxide from two adjacent OH-terminations) can be reactivated. It follows that when the SiNCs are dispersed in water, H-terminations and any existing Si-dimer will progressively be replaced by Si-oxide (Si–O–Si or Si=O) through OH-condensation. In some cases, OH-terminations that remain isolated will not progress into condensation and therefore may become deprotonated giving a characteristic negative surface charge (measured zeta potential < –30 mV). These surface states have been previously confirmed by FTIR[27] and correspond to the high PL intensity region of Figure 3c,e (<20 h storage in water) whereby any dangling bonds or strained Si-bonds/dimers are removed and allow increasing transitions via carriers that are trapped in oxide-related surface localized states. Nonetheless, after 20 h and up to 40 h of water exposure (Figure 3c,e), the condensation process (two adjacent Si–O–H that produce Si-oxide and water) necessarily leaves behind further defects and strained bonds that are susceptible to further water cleavage[48] and allow for the oxidation to progress inward. While oxygen-based passivation that is restricted to the outermost layer can improve PL intensity by reducing surface defects, inward oxide growth increases defects density and therefore provides non-radiative recombination paths for electron–hole pairs with consequent decreased PL at the oxide localized states. The corresponding PL blue-shift during 20–40 h storage may be due the progressive reduction of the

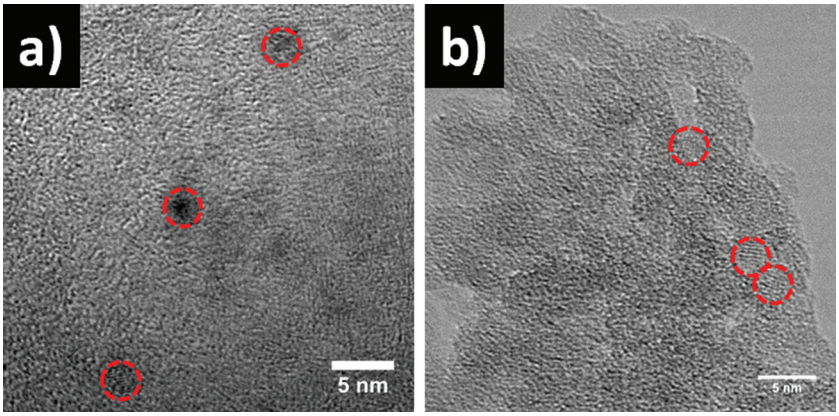

Figure 4. Corresponding TEM images of SiNCs produced by electrochemical etching and then stored in water (a,b) and in ethanol (c,d) for several weeks.

Si-core diameter.[4] It can be said that the 20–40 h storage period marks the transition from surface chemistry, restricted to a few surface monolayers, to chemical reactions that may involve up to 1–2 nm shell thicknesses of the SiNCs. Finally, after 40 h that the SiNCs have been stored in water, both PL intensity and the peak wavelength are stabilized; the plateau after 40 h storage may be due to diffusion limitations that prevent the oxide growth as well as due to the emission being solely produced at the oxide-related surface states, where the emission effectively "locks" just below 600 nm.[4] In fact, the PL maximum around 575 nm is consistent with oxygen-related localized recombination in nanocrystals with diameter below 3 nm.[4]

The TEM images (**Figure 4**) are also in support of this analysis. TEM image (Figure 4a) of the W/SiNCs shows that the crystal structure is still present but the sample has lost the particulate pattern and shows a more uniform, possibly amorphous Si-oxide material. Also, the SiNCs that can be observed in Figure 4a are clearly smaller (≈2.5 nm diameter) than those that were observed in Figure 2c, consistent with the core reduction due to the growth of an oxide shell.

The time-dependent PL measurements for Et/SiNCs exhibit very similar trends if compared to W/SiNCs. It can be noticed that the exponential decay in the PL intensity for the Et/SiNCs (Figure 3d) is the same as the one observed in Figure 3c for W/SiNCs, where the first is somewhat slower; the PL intensity in W/SiNCs decreases below 10% of its maximum only after ≈35 h while in Et/SiNCs it takes ≈50 h for the PL intensity to be reduced to less than 10% of its maximum. The region of high PL intensity that was observed below 20 h in W/SiNCs (Figure 3c), is now extended to the first 25 h for Et/SiNCs (Figure 3d). The decay of the PL intensity for Et/SiNCs occurs from 25 h up to 50 h of ethanol exposure (versus 20–40 hours for W/SiNCs). A similar analysis can be conducted for the blue shift (Figure 3e,f) where Et/SiNCs exhibits the same trend as it was observed for W/SiNCs but over a longer period, which may indicate that the same surface chemistry is taking place in both colloids but at different rates, faster for W/SiNCs and slower for Et/SiNCs. TEM images of Et/SiNCs are reported in Figure 4b; although the images do not allow a precise quantitative analysis, the Et/SiNCs sample of Figure 4b have preserved to a larger extent the particulate pattern and with SiNCs that may appear slightly larger than those found in Figure 4a.

Therefore, direct contact of SiNCs with ethanol does not induce any surface chemistry and it is believed that changes in Et/SiNCs are only due to water-induced oxidation from water vapor dissolved in ethanol from ambient air (see Supporting Information for evidence of water vapor dissolving in ethanol). Et/SiNCs present a lower water concentration compared to W/SiNCs and are therefore subject to slower surface reaction rates.

2.3. Microplasma-Induced Non-Equilibrium Liquid Chemistry (MiNE-LC) of SiNCs in Water or Ethanol and their Optical Properties

In the previous section we have shown that the optical properties of SiNCs can degrade very easily in liquids and particular attention has to be paid to preserve surface characteristics. Chemical routes,[2,13,23,24] UV irradiation,[9] low-pressure plasmas,[54] or laser-based techniques[14,28,31] have already been used to provide organic-/oxide-based surface terminations. We have explored here the possibility of using atmospheric pressure microplasmas to engineer the surface of SiNCs so that these could be easily stored and manipulated in liquids without constraints due to water or water vapor. The microplasma-based process presented here has unique features with the potential to extend accurate control of SiNCs surface engineering to a wide range of termination types including organic and inorganic materials.[22,29,33,55]

The microplasma setup (**Figure 5**) allows for the generation of an atmospheric-pressure microplasma at the surface of a liquid (see Experimental Section and ref. [29] for more details).

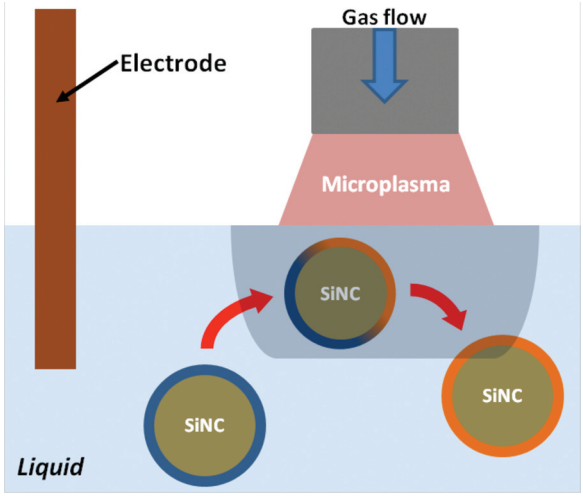

Figure 5. Schematic diagram of the microplasma process. SiNCs are subject to microplasma-induced liquid chemistry that modifies the surface characteristics. The microplasma requires a gas flow and a counter electrode immersed in the liquid.

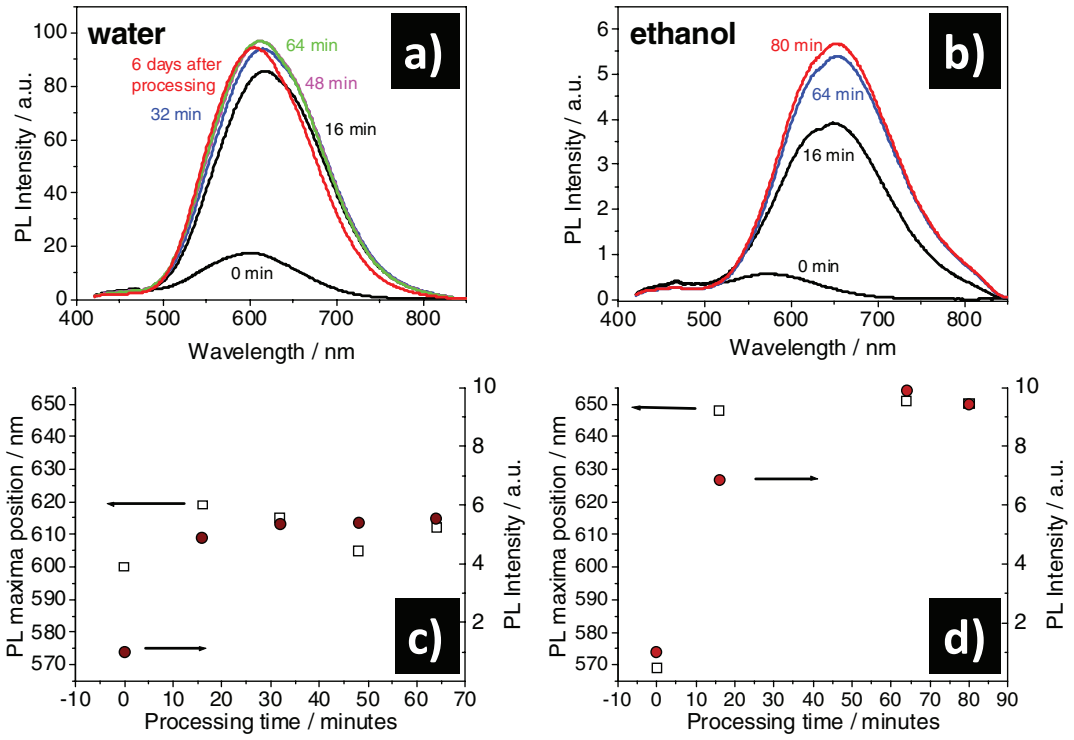

Figure 6. PL spectra of SiNCs dispersed in water (a) and in ethanol (b) before and after microplasma processing at different processing time. Summary of PL intensity maxima (open circles) and corresponding wavelengths (full black squares) vs. microplasma processing time for both SiNCs colloids in water (c) and in ethanol (d).

Electrons from the plasma are injected through the plasma/liquid interface forming a liquid volume with very high electron densities (≈10^{19} m^{-3})[22] and inducing a chain of chemical reactions in the liquid phase (darker blue area under the microplasma of Figure 5). MiNE-LC differs from standard electrochemistry or radiolysis because of the following main points: a) MiNE-LC produces a high concentration of electrons in the liquid phase that would not be achievable in standard electrochemistry or by radiolysis techniques;[56] b) MiNE-LC relies on highly non-equilibrium kinetically-driven reactions; c) in MiNE-LC, reactions at the liquid surface are electrode-less, preventing any deposition to occur or any other electrode surface chemistry to interfere; and d) in MiNE-LC, both the number density as well as the kinetic energy of the electrons reaching the liquid surface may contribute to control the chemical reactions.[33] The configuration described here also allows controlled electron-driven plasma–liquid interactions whereby most of the induced liquid chemistry is determined by the electrons "injected" from the plasma into the liquid. It has been shown that photons and other gas-phase radicals have very limited effect in this type of microplasma process.[55]

MiNE-LC has been used here to treat both W/SiNCs and Et/SiNCs. As before, colloids made of 5 mg of SiNCs powder and 20 mL of water (or ethanol) were produced and left to settle for about 15 min, then 10 mL of the supernatant parts were separated and used immediately for microplasma processing. **Figure 6** compares PL spectra of W/SiNCs (Figure 6a) and Et/SiNCs (Figure 6b) before and after microplasma processing at different processing time. For both colloids, significant changes in PL properties are recorded as a function of processing time. The plots of Figure 6c,d summarize the PL maxima wavelengths (open symbols) and PL maxima intensities (full symbols) for W/SiNCs and Et/SiNCs at different microplasma processing times. In both colloids the PL intensity has increased. However, the PL maximum of microplasma-treated W/SiNCs exhibit a small red shift (≈12 nm) while a much larger red shift (≈80 nm) is observed for Et/SiNCs. Importantly, microplasma processing resulted in considerable improvements in the SiNCs stability where both colloids preserve the same PL properties for several days after microplasma processing. The emission recorded for the W/SiNCs six days after microplasma processing is shown in Figure 6a (red line) and no significant change in the PL maximum intensity/wavelength is observed. Et/SiNCs have shown also stability of PL properties and these will be discussed in more details in the next section. It has to be noted that PL changes are specific to the microplasma treatment given that standard electrochemistry at similar conditions did not produce the same results (see Supporting Information for more details).

TEM images show that after microplasma processing and several days storage in water (**Figure 7**a,c) or ethanol (Figure 7b,d), the SiNCs have preserved the initial size of about ≈4 nm, which confirms that microplasma processing has prevented the oxide growth due to water. In both cases the crystalline nature can be still observed. The SiNCs processed in ethanol also exhibit improved dispersion on the TEM grid, which may be related to the surface functionalization that will be discussed in the next section.

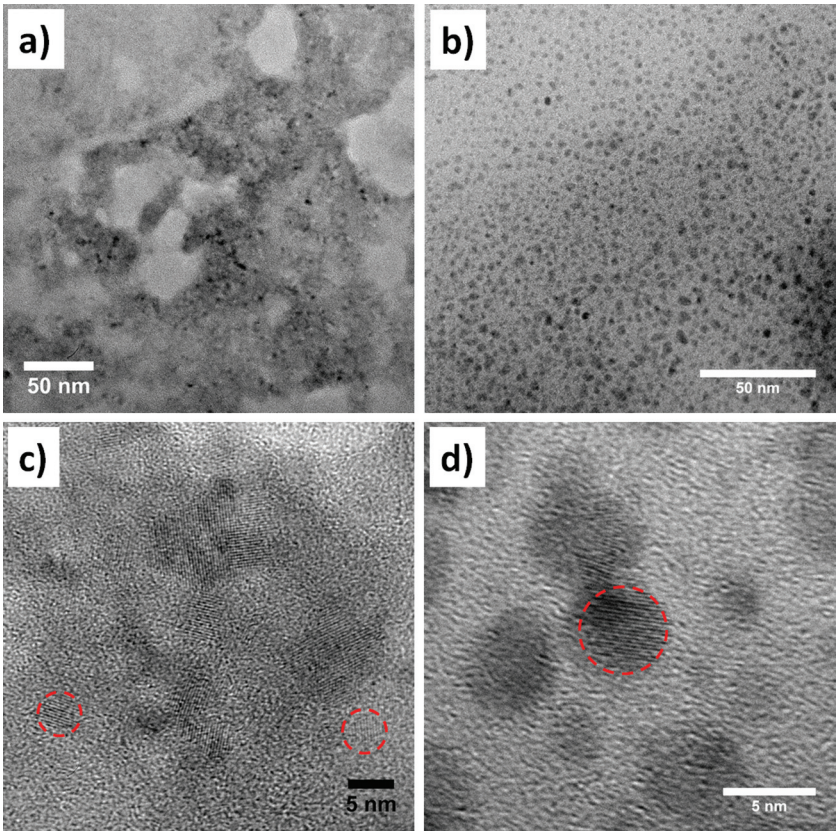

Figure 7. Low (a,b) and high (c,d) magnification TEM images of microplasma-treated SiNCs processed in water (a,c) and in ethanol (b,d).

This type of microplasma processing techniques is a very new and unique approach to surface engineering of SiNCs. The chemical reactions induced by the microplasma–liquid interactions are still under investigation[33,36,57] and theoretical simulation would require hybrid models that can couple plasma chemistry with non-equilibrium wet chemistry. Microplasma processing in water is very likely to initiate hydrolysis where the high electron densities can generate a large number of OH^- ions ($2H_2O + 2e^- \rightarrow 2OH^- + H_2$). Hydroxide anions can then induce surface chemistry on the SiNCs as previously discussed for SiNCs stored in water; however we speculate that due to the high concentration of ions, the oxidation process results in a fast and complete surface-restricted passivation that prevents and protects the SiNCs from any further reactions directed inward towards the nanocrystals core. This justifies the PL maximum at about 615 nm in Figure 6c, which was observed also for SiNCs stored in water (Figure 3e) and associated to trapped oxide surface states. Contrary to Figure 3e, microplasma-treated SiNCs in water do not undergo degradation of the PL properties (Figure 6a, red curve) due to the fast and full surface-limited oxidation. In summary, microplasma processing in water produces the same molecular radicals/ions that could be found during water storage but reaction kinetics occurs at a much faster rate due to the much higher OH^- concentrations, which limit chemical reactions to the outmost surface layers.

In ethanol, microplasma processing can however induce a completely different chemistry, with the formation of molecular radicals that would not normally be present in ethanol or water. For this reason we will now focus on the analysis of MiNE-LC in ethanol.

2.4. Stability and Surface Characteristics of Microplasma-Treated SiNCs in Ethanol

Similarly to the previous section (Figure 6b,d), we have repeated MiNE-LC several times for Et/SiNCs and we have monitored the effect of storage in ethanol of the microplasma-treated SiNCs for several days; however in this case we used a higher initial concentration of SiNCs (≈15 mg in 20 mL of ethanol) and the supernatant 10 mL have been used for microplasma processing.

Figure 8 shows PL intensity and maxima for different samples, at different processing times and for several days of storage in ethanol after microplasma treatment. A strong red-shift is observed for microplasma-treated SiNCs which mainly occurs within the first 20 min treatment (Figure 8a). The red-shift stabilizes at ≈650 nm and remains stable for several days after processing (Figure 8b). The PL intensity on the other hand increases almost linearly with processing time (Figure 8c) and it is observed to increase slightly with storage in ethanol (Figure 8d); it should be noted that the timescale of Figure 8d is much longer than that of Figure 8c.

The FTIR spectrum of **Figure 9** can be used to analyze the specific surface terminations after microplasma processing of the Et/SiNCs. The SiNCs powder was dispersed in ethanol shortly before microplasma processing; therefore the surface characteristics at the beginning of the microplasma treatment are very similar to those in Figure 1 as insufficient time was given for water vapor in ethanol to induce the surface chemistry that was previously discussed. By comparing Figure 1 with Figure 9, it can be said that the microplasma treatment has completely removed all H-terminations as no absorption related to Si–H bonds is observed in the ranges 2000–2250 cm^{-1}, 600–700 cm^{-1}, and at 916 cm^{-1} (Si–F bonds with corresponding absorption at 930 cm^{-1} have been also removed). Instead aliphatic stretching corresponding to C–H bonds is detected between 2800 cm^{-1} and 3000 cm^{-1}.[2,13,44,49,58] Given the predominance of peaks located around 2916 cm^{-1}, 2932 cm^{-1}, and 2875 cm^{-1},[49,58] the origin of these bands can be assigned mainly to $C–H_2$ stretching and in minor part to $C–H_3$. A related absorption band is found between 1300 cm^{-1} and 1450 cm^{-1}; also in this case absorption is assigned to $C–H_x$ modes.[7,13,44,49,58] The broad absorption between 3000 cm^{-1} and 3750 cm^{-1} is due to O–H and it could originate from both SiO–H and CO–H. The absorption between 1000 cm^{-1} and 1250 cm^{-1} is quite important because within this range both Si–O and C–O have active modes. The strong peak just above 1050 cm^{-1} is generally due to Si–O–Si stretching and compared to the dry SiNCs powder

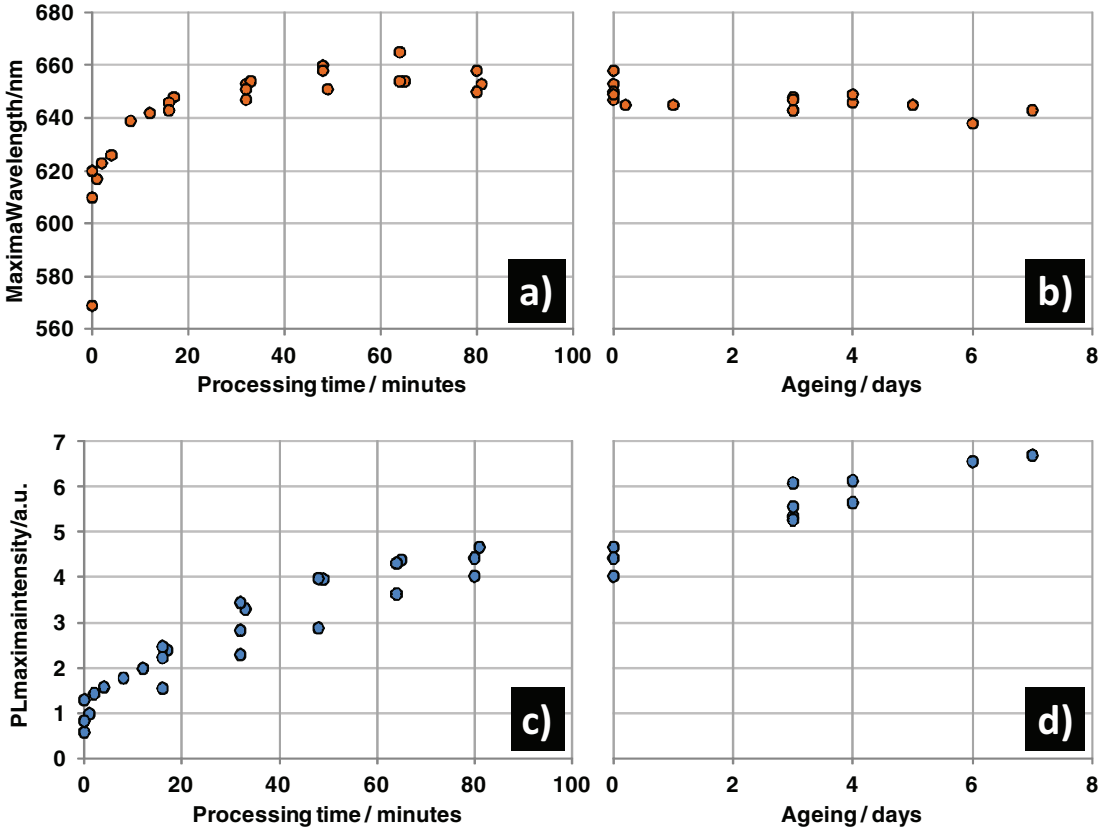

Figure 8. PL maxima wavelength (a) and intensity (c) of SiNCs in ethanol before and after microplasma processing at different processing time. b,c) Effect of storage in ethanol after microplasma processing for several days.

(Figure 1), the peak has narrowed and shifted towards higher wavenumbers. The shoulder from 1150 cm^{-1} to 1250 cm^{-1} can be assigned to C–O stretching[24] and a minor peak at about 1040 cm^{-1} could be due to Si–O–C.[7] The presence of C–O bonds indicates that organic molecules have attached to the SiNCs surface through oxygen atoms forming Si–O–R terminations. This type of termination could justify the shape and position of the peak at ≈1050 cm^{-1}: if the SiNCs surface is well passivated, a large contribution to the absorption peak comes from stretching of the oxygen atom within the Si–O–C bonds contributing to a narrow distribution.[51] The peak position is close to the stochiometric Si–O–Si stretching at 1075 cm^{-1},[51] as it could be expected by complete Si–O–R passivation where the lower wavenumber may be due to the carbon atoms replacing the silicon atoms in Si–O–Si. This is confirmed by the absence of the Si–O–Si bending mode at about 800 cm^{-1},[52] as this would not be observed in Si–O–R terminations. The peak at ≈1590 cm^{-1} is due to C=C stretching[2,24,44] or C–C.[44] It should be added that absorption bands related to Si–C at 677 cm^{-1}, 750 cm^{-1}, 852 cm^{-1}, and 2357 cm^{-1} are not detected.[7,44]

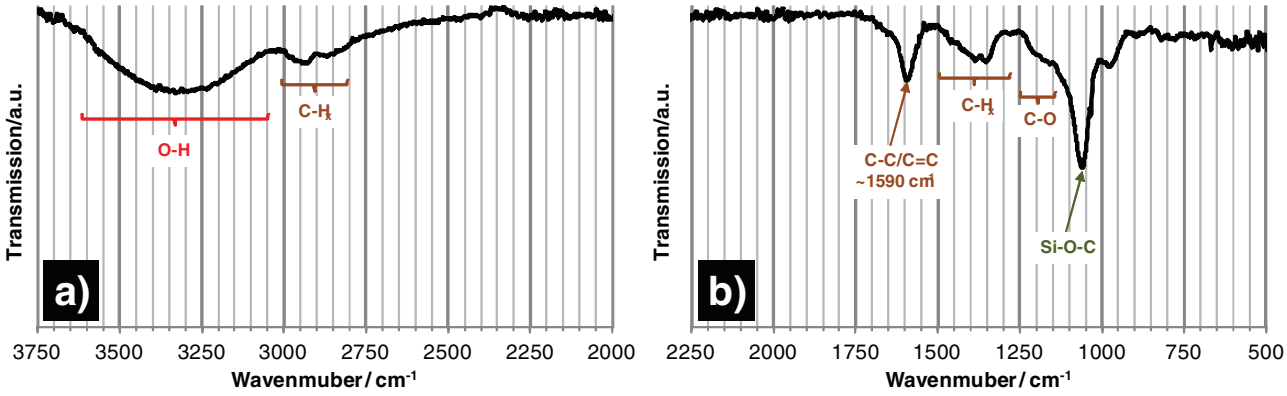

Figure 9. FTIR spectrum of the microplasma treated SiNCs in ethanol. a) FTIR signal from 3750 cm^{-1} to 2000 cm^{-1} and b) FTIR signal of the same sample in the range 2250–500 cm^{-1}.

From these observations, it is clear that SiNCs under microplasma processing have undergone a surface modification whereby Si–H bonds and other surface terminations (Figure 1) have been removed and replaced completely by Si–O–R terminations. Several chemical groups that are not contradictory to the FTIR measurements are possible and we are currently unable to identify the specificity of the Si–O–R terminations. It is likely that Si–OH terminations exist on the surface of the SiNCs, however these are very likely to condensate and therefore we believe that hydroxyl groups which are responsible for the absorption above 3000 cm^{-1} are contained in the Si–O–R terminations, i.e., Si–O–R–$(OH)_x$. Furthermore, the stronger absorption from C–H_2 may suggest that a likely termination could be of the type Si–O–CH_2–CH_2–OH.

This FTIR analysis can also explain the PL measurements of Figure 8 (and also of Figure 6b,d). While the Et/SiNCs is being treated by the microplasma, two types of SiNCs can be found in the solution: those that have not come in contact yet with reactive species and those that have interacted with radicals and therefore have been subject to surface modifications (see Figure 5), where the surface-modified SiNCs progressively increase in number at the expenses of the "untreated" SINCs. "Untreated" SiNCs are negatively charged (the measured zeta potential is below –30 mV) and travel to the microplasma/liquid interface by electrophoresis,[59] while "treated" SiNCs (zeta potential is higher than –10 mV after 90 min processing) diffuse out of the reaction zone. Untreated SiNCs possess characteristics that resemble those of the SiNCs powder in ethanol and with time, they will follow optical properties similar to those measured in Figure 3d,f. These untreated SiNCs contribute to a moderate increase in PL emission intensity with an almost immediate shift from ≈570 nm to above 600 nm (see Figure 3f). This is consistent with Figure 8a and Figure 6c where, within the first few minutes, the PL intensity is increased and the PL maximum shifts to above 600 nm. However these untreated SiNCs decrease in number as the microplasma-induced reactions provide surface passivation to an increasing number of SiNCs. At this time the PL emission of the treated SiNCs dominates so that after 20 min processing, PL emission is only due to Si–O–R passivated SiNCs. The PL intensity increases linearly with processing time because it only relates to the increasing number of passivated SiNCs and it can be noticed that for lower SiNCs concentration (Figure 6d), the intensity increases more rapidly with processing time. The PL emission wavelength at about 650 nm is stable because it originates only from fully Si–O–R passivated SiNCs, while the emission at 605 nm of the untreated SiNCs hides in the background; at lower SiNCs concentrations (Figure 6d), exactly the same behavior was observed and confirms that this can be associated to the surface treated SiNCs. The PL emission at 650 nm for the Si–O–R passivated SiNCs can be justified by oxygen-/organic-based surface reconstruction, limited at the outer monolayer of the SiNCs.[10,60]

2.5. Analysis of MiNE-LC Processes in Ethanol

In this final section we provide a possible description of the microplasma-induced reactions in the specific case of microplasma-treated Et/SiNCs. Electron number densities in atmospheric-pressure microplasmas can reach up to ≈10^{21} m^{-3},[22] and for this dc microplasma, a number density in the range of 10^{18} m^{-3} can be expected. Due to the conservation of the electric displacement field, at the plasma/liquid interface, the electron number density can increase by two orders of magnitude so that within a few micrometer of depth in the liquid (typical diffusion length of solvated electrons[56]) electron number densities can be 10^{20} m^{-3}. While electrons will tend to react very rapidly and their lifetime is likely very limited, this very high concentration of electrons injected in the liquid from the plasma creates a highly non-equilibrium zone with electrons that can drive reaction kinetics and induce dissociation of the hydrogen atom at the hydroxyl-end of the ethanol molecules, i.e., producing $CH_3CH_2O^-$ ions[56] (**Figure 10**a). These radicals can easily react with any termination at the SiNCs surface and,

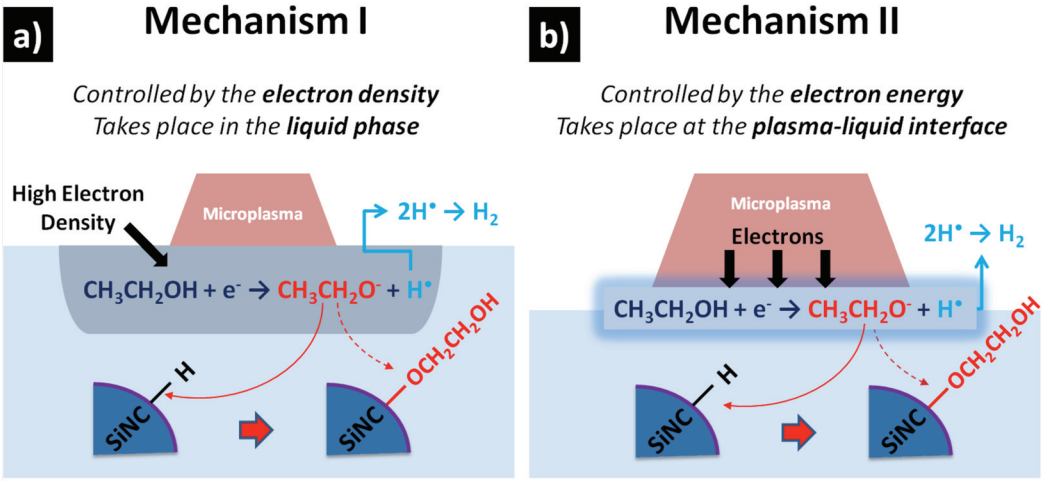

Figure 10. Schematic diagrams describing two possible mechanisms for dissociation of ethanol molecules, one determined by the high electron concentration in the colloid (a) and the second determined by dissociative electron attachment and therefore depending on the electron energy (b). A similar type of reaction is possible for water (not shown) where H_2O dissociates in OH^- and H radical; in the specific context discussed in the text, hydroxide anions have reacted with the Si–O–R terminations.

in particular, can replace Si–H termination with Si–O–C_2H_5. This is probably the most likely reaction path that explains the replacement of H-terminations with Si–O–R (see FTIR in Figure 9). The large O–H absorption above 3000 cm^{-1} (Figure 9a) is likely due to CO–H (and not SiO–H) produced by the reaction of the OH^- ions with the Si–O–R group forming Si–O–R–$(OH)_x$ terminations. This provides an explanation for the FTIR signal of Figure 9 and is consistent with Si–O–R–$(OH)_x$ terminations, as previously argued.

While these types of reactions are all determined by the high concentrations of electrons in ethanol (see Figure 10a, mechanism I), a second mechanism may be possible where a key role is played by the kinetic energy of electrons reaching the liquid surface from the plasma. In this second mechanism (Figure 10b, mechanism II), electrons from the gas phase can induce dissociative electron attachment (DEA) when they come in contact with the liquid surface. DEA is an energy-dependent reaction where electrons can determine the detachment of particular fragments depending on their kinetic energy; for instance detachment of H^- ions exhibit higher yields at about 6.4 eV electron energy[61] while OH^- detachment is resonant at ≈8 eV.[62] In this case, depending on the electron energy distribution function at the plasma/liquid interface, DEA can contribute to the formation of a range of molecular fragments from ethanol molecules and it is possible that at some extent these are all present with varying concentrations. While either type of reaction paths, electron density dependent or electron energy dependent (i.e., DEA), can explain our experimental results of the microplasma process, it is likely that both mechanisms are playing a role in the surface functionalization of the SiNCs in ethanol. At this time we cannot provide experimental evidence to support which one of the mechanisms is more important, but we believe that this represents an exciting area of research that can provide the possibility of achieving superior control over plasma-activated wet chemistry.[33]

3. Conclusions

We have provided important experimental results that relate to the time-dependent evolution of optical properties when SiNCs are stored in water or in ethanol. The experimental details discussed are of particular importance for the future implementation of silicon-based quantum dots in various applications where liquid-based storage and manipulation are fundamental steps. We have then produced details of a novel microplasma-based approach that has been used to stabilize SiNCs surface characteristics in water and ethanol. In particular, microplasma processing is a low-cost and scalable technique with the potential of being extended to a wide range of organic and inorganic materials. The optical properties of SiNCs that have been treated with the microplasma have shown to be stable over several days of storage in water or ethanol.

Finally, a more in-depth analysis has been produced for the Et/SiNCs where SiNCs have acquired an organic functionalization. Microplasma processing clearly enhances the SiNCs PL intensity and stability and it red-shifts the PL maximum. An analysis of the microplasma-induced reactions indicates that microplasma processing may offer great opportunities and can greatly contribute to achieve superior control of nanomaterial interfaces, which represent one of the next most important challenges for a wide range of nanotechnology applications.

4. Experimental Section

Description of the Electrochemical Etching Process: Similarly to previous work,[31] the powder containing single SiNCs and SiNCs clustered up to micrometer-sized aggregates was produced by electrochemical etching of a silicon wafer (p-type boron doped, <100>, 0.1 Ω cm, thickness 0.525 mm) and subsequent mechanical pulverization.[18,26] A solution of ethanol/HF (50:50 concentration) was used for electrochemical etching and a 2.5 cm diameter area of the wafer surface was exposed to etching. A current density of 3 mA cm^{-2} was applied via a carbon electrode (cathode, 5 mm diameter) immersed in the solution ≈3 cm away and above the silicon wafer.

Microplasma-Induced Non-Equilibrium Liquid Chemistry (MiNE-LC): Similarly to previous work,[29] a dc atmospheric-pressure microplasma was generated between a Ni tubing (inner diameter 0.7 mm, outer 1 mm) and the surface of the SiNCs colloid. As a counter electrode, a carbon rod (5 mm diameter) was immersed about 5 mm in the solution at a distance of about 3 cm from the nickel tubing. A positive voltage was applied to the carbon rod while the nickel tubing was connected to ground through a 100 kΩ resistor. Pure argon was flown inside the Ni tubing at a rate of 25 sccm. The distance between the nickel tubing and the liquid dispersion surface was initially adjusted at 1 mm, however during processing the distance was observed to increase to about 1.3–1.5 mm (about every ≈15 min processing) due to evaporation particularly seen in the case of ethanol. The temperature of the colloids did not increase above 38 °C within ≈15 min processing time. During the microplasma treatment, the conductivity of the colloid was also observed to change as applying the same voltage the current would tend to increase slowly. Therefore the applied voltage was initially set at 2 kV until the current reached 1.5 mA and subsequently the voltage was adjusted to keep the current constant at 1.5 mA. After about 90 min processing the applied voltage required to produce a constant current of 1.5 mA was about 800 V.

Photoluminescence Measurements: The PL measurements were carried out at room temperature directly from the colloids. The PL was measured with a Xe lamp (FluoroMax-4 Spectrofluorometer) and an excitation at 400 nm was used.

FTIR Analysis: For FTIR spectroscopy (Perkin-Elmer Spectrum 2000) analysis, the colloids were drop-cast and dried on a silicon wafer; analysis of the dry powder was achieved by simply depositing a small amount of the powder on the silicon substrate. FTIR measurements were taken in ratio mode using as reference a section from the same silicon wafer where the SiNCs were deposited. The range 370–7800 cm^{-1} was scanned with a resolution of 1 cm^{-1} and 0.2 cm^{-1} steps.

Supporting Information

Supporting Information is available from the Wiley Online Library or from the author.

Acknowledgements

This work was partially supported by a NEDO Project (Japan). D.M. gratefully acknowledges the support of the JSPS Invitation Fellowship (Japan) and discussions with Dr. S. Cook and Dr. H. Mizuno (AIST, Japan). The TEM analysis was supported by the Science Foundation Ireland National Access Programme (Project n. 283).

Received: September 6, 2011
Published online: December 19, 2011

[1] N. Koshida, *Device Applications of Silicon Nanocrystals and Nanostructures*, Springer Science+Business Media, New York **2008**.
[2] F. Hua, F. Erogbogbo, M. T. Swihart, E. Ruckenstein, *Langmuir* **2006**, *22*, 4363.
[3] J. Zou, R. K. Baldwin, K. A. Pettigrew, S. M. Kauzlarich, *Nano Lett.* **2004**, *4*, 1181.
[4] M. W. Wolkin, J. Jorne, P. M. Fauchet, G. Allan, C. Delerue, *Phys. Rev. Lett.* **1999**, *82*, 197.
[5] D. Timmerman, I. Izeddin, P. Stallinga, I. N. Yassievich, T. Gregorkiewicz, *Nat. Photonics* **2008**, *21*, 105.
[6] W. D. A. M. de Boer, D. Timmerman, D. Dohnalová, I. N. Yassievich, H. Zhang, W. J. Buma, T. Gregorkiewicz, *Nat. Nanotechnol.* **2010**, *5*, 878.
[7] K. Kusová, O. Cibulka, K. Dohnalova, I. Pelant, J. Valenta, A. Fucikova, K. Zidek, J. Lang, J. Englich, P. Matejka, P. Stepanek, S. Bakardjieva, *ACS Nano* **2010**, *4*, 4495.
[8] D. J. Binks, *Phys. Chem. Chem. Phys.* **2011**, *13*, 12693.
[9] J. A. Kelly, J. G. C. Veinot, *ACS Nano* **2010**, *4*, 4645.
[10] R. Guerra, E. Degoli, S. Ossicini, *Phys. Rev. B* **2009**, *80*, 155332.
[11] L. Pavesi, D. Lockwood, *Silicon Photonics*, Springer, Berlin, Germany **2004**.
[12] D. Kovalev, M. Fujii, *Adv. Mater.* **2010**, *17*, 2531.
[13] C. M. Hessel, M. R. Rasch, J. L. Hueso, B. W. Goodfellow, V. A. Akhavan, P. Puvanakrishnan, J. W. Tunnel, B. A. Korgel, *Small* **2010**, *6*, 2026.
[14] V. Švrček, D. Mariotti, T. Nagai, Y. Shibata, I. Turkevych, M. Kondo, *J. Phys. Chem. C* **2011**, *115*, 5084.
[15] M. C. Beard, K. P. Knutsen, P. Yu, J. M. Luther, Q. Song, W. K. Metzger, R. J. Ellingson, A. J. Nozik, *Nano Lett.* **2007**, *8*, 2506.
[16] C.-Y. Liu, Z. Holman, U. Kortshagen, *Nano Lett.* **2009**, *9*, 449.
[17] V. Švrček, D. Mariotti, Y. Shibata, M. Kondo, *J. Phys. D: Appl. Phys.* **2010**, *43*, 415402.
[18] V. Švrcek, A. Slaoui, J.-C. Muller, *J. Appl. Phys.* **2004**, *95*, 3158.
[19] R. M. Sankaran, D. Holunga, R. C. Flagan, K. P. Giapis, *Nano Lett.* **2005**, *5*, 537.
[20] T. Nozaki, K. Sasaki, T. Ogino, D. Asahi, K. Okazaki, *Nanotechnology* **2007**, *18*, 235603.
[21] U. Kortshagen, *J. Phys. D: Appl. Phys.* **2009**, *42*, 113001.
[22] D. Mariotti, R. M. Sankaran, *J. Phys. D: Appl. Phys.* **2010**, *43*, 323001.
[23] J. D. Holmes, K. J. Ziegler, R. C. Doty, L. E. Pell, K. P. Johnston, B. Korgel, *J. Am. Chem. Soc.* **2001**, *123*, 3743.
[24] S. Sato, M. T. Swihart, *Chem. Mater.* **2006**, *18*, 4083.
[25] S. Y. Huang, A. D. Arulsamy, M. Xu, S. Xu, U. Cvelbar, M. Mozetic, K. Ostrikov, *Phys. Plasmas* **2009**, *16*, 123504.
[26] I. Levchenko, K. Ostrikov, D. Mariotti, V. Švrček, *Carbon* **2009**, *47*, 2379.
[27] V. Švrček, D. Mariotti, K. Kalia, C. Dickinson, M. Kondo, *J. Phys. Chem. C* **2011**, *115*, 6235.
[28] V. Švrček, D. Mariotti, M. Kondo, *Opt. Express* **2009**, *17*, 520.
[29] V. Švrček, D. Mariotti, M. Kondo, *Appl. Phys. Lett.* **2010**, *97*, 161502.
[30] I. Levchenko, K. Ostrikov, D. Mariotti, *Carbon* **2008**, *47*, 313.
[31] V. Švrček, M. Kondo, K. Kalia, D. Mariotti, *Chem. Phys. Lett.* **2009**, *478*, 224.
[32] D. Mariotti, V. Švrček, D.-G. Kim, *Appl. Phys. Lett.* **2007**, *91*, 183111.
[33] D. Mariotti, R. M. Sankaran, *J. Phys. D: Appl. Phys.* **2011**, *44*, 174023.
[34] T. Belmonte, T. Gries, R. P. Cardoso, G. Arnoult, F. Kosior, G. Henrion, *Plasma Sources Sci. Technol.* **2011**, *20*, 024004.
[35] T. Belmonte, G. Henrion, T. Gries, *J. Therm. Spray Technol.* **2011**, *20*, 744.
[36] D. Mariotti, Y. Shimizu, T. Sasaki, N. Koshizaki, *Appl. Phys. Lett.* **2006**, *89*, 201502.
[37] D. Mariotti, A. C. Bose, K. Ostrikov, *IEEE Trans. Plasma Sci.* **2009**, *37*, 1027.
[38] D. O'Connell, L. J. Cox, W. B. Hyland, S. J. McMahon, S. Reuter, W. G. Graham, T. Gans, F. J. Currell, *Appl. Phys. Lett.* **2011**, *98*, 043701.
[39] K. Ostrikov, U. Cvelbar, A. B. Murphy, *J. Phys. D: Appl. Phys.* **2011**, *44*, 174001.
[40] R. Reuter, D. Ellerweg, A. von Keudell, J. Benedikt, *Appl. Phys. Lett.* **2011**, *98*, 111502.
[41] L. Pavesi, R. Turan, *Silicon Nanocrystals: Fundamentals, Synthesis and Applications*, Wiley-VCH, Weinheim, Germany **2010**.
[42] Y. Kanemitsu, H. Uto, Y. Masumoto, T. Matsumoto, T. Futagi, H. Mimura, *Phys. Rev. B* **1993**, *48*, 2827.
[43] Y. H. Ogata, N. Yoshimi, R. Yasuda, T. Tsuboi, T. Sakka, A. Otsuki, *J. Appl. Phys.* **2001**, *90*, 6487.
[44] D. Xu, L. Sun, H. Li, L. Zhang, G. Guo, X. Zhao, L. Gui, *New J. Chem.* **2003**, *27*, 300.
[45] N. Prtljaga, E. D'Amato, A. Pitanti, R. Guider, E. Froner, S. Larcheri, M. Scarpa, L. Pavesi, *Nanotechnology* **2011**, *22*, 215704.
[46] D. C. Marra, E. A. Edelberg, R. L. Naone, E. S. Aydil, *J. Vac. Sci. Technol. A* **1998**, *16*, 3199.
[47] X. H. Sun, S. D. Wang, N. B. Wong, D. D. D. Ma, S. T. Lee, B. K. Teo, *Inorg. Chem.* **2003**, *42*, 2398.
[48] Y. H. Ogata, F. Kato, T. Tsuboi, T. Sakka, *J. Electrochem. Soc.* **1998**, *145*, 2439.
[49] N. Y. Kim, P. E. Laibinis, *J. Am. Chem. Soc.* **1999**, *121*, 7162.
[50] J.-S. Chou, S.-C. Lee*J. Appl. Phys.* **1995**, *77*, 1805.
[51] P. G. Pai, S. S. Chao, Y. Takagi, G. Lucovsky, *J. Vac. Sci. Technol. A* **1986**, *4*, 689.
[52] G. Lucovsky, M. J. Manitini, J. K. Srivastava, E. A. Irene, *J. Vac. Sci. Technol. B* **1987**, *5*, 530.
[53] Y. Borensztein, O. Pluchery, N. Witkowski, *Phys. Rev. Lett.* **2005**, *95*, 117402.
[54] L. Mangolini, U. Kortshagen, *Adv. Mater.* **2007**, *19*, 2513.
[55] S. W. Lee, D. Liang, X. P. A. Gao, R. M. Sankaran, *Adv. Funct. Mater.* **2011**, *21*, 2155.
[56] B. H. Milosavljevic, O. I. Micic, *J. Phys. Chem.* **1987**, *82*, 1360.
[57] P. Bruggeman, *J. Phys. D: Appl. Phys.* **2009**, *42*, 053001.
[58] A. Grill, D. A. Neumayer, *J. Appl. Phys.* **2003**, *94*, 6697.
[59] V. Švrček, I. Turkevych, K. Hara, M. Kondo, *Nanotechnology* **2010**, *21*, 215203.
[60] R. Guerra, S. Ossicini, *Phys. Rev. B* **2010**, *81*, 245307.
[61] V. S. Prabhudesai, D. Nandi, A. H. Kelkar, E. Krishnakumar, *J. Chem. Phys.* **2008**, *128*, 154309.
[62] M. Orzol, I. Martin, J. Kocisek, I. Dabkowska, J. Langer, E. Illenberger, *Phys. Chem. Chem. Phys.* **2007**, *9*, 3424.